Nuclear Electric Propulsion Modular Power Conversion Model

Dennis Nikitaev[1], Corey D. Smith[1], Matthew Duchek[2], Christopher Harnack[2], William Machemer[2], and Emanuel Grella[2]

Advanced Projects Huntsville, Analytical Mechanics Associates, Huntsville, AL, 35806
Advanced Projects Denver, Analytical Mechanics Associates, Denver, CO, 80211

Primary Author Contact Information: 702-287-6852, dennis.d.nikitaev@ama-inc.com

DOI: ####

This work builds upon a previously examined single loop power conversion cycle for nuclear electric propulsion systems. The intent of this model is to enable examination of trends within the system and extract system parameters that could be used in a mass model to understand how technology performance may impact overall system mass. Several model upgrades were made since the previous work which included physics-based sizing of the turbomachinery and pressure loss inside the radiator. A higher fidelity and modular fluid property code was also developed to help understand the impact of variable fluid properties more accurately and allow for the analysis of different fluids in the same model. The upgraded model features radiator and reactor loops with separate fluids from the Brayton cycle to understand advantages and disadvantages of using multiple working fluids as well as the capability of simulating off nominal system performance. The latter provides a steppingstone for modeling the transient performance of the power conversion system.

I. INTRODUCTION

Currently, NASA is considering both Nuclear Electric Propulsion (NEP) and Nuclear Thermal Propulsion (NTP) as potential technologies for a crewed mission to Mars. Electric propulsion systems that have been flight tested relied on solar energy. Solar Electric Propulsion (SEP) has been used in small spacecraft and space exploration probes such as the BepiColombo mission to Mercury[1] while NTP was ground tested by project ROVER and the Nuclear Engine for Rocket Vehicle Application (NERVA) program[2]. The Systems for Nuclear Auxiliary Power 10A (SNAP-10A) was the world's first nuclear reactor in space as well as the first NEP system since the reactor powered an ion thruster system in orbit resulting in NEP being flight tested. The key differences between NEP and NTP are the level of thrust produced and the specific impulse. Current electric propulsion technologies that have been grounded tested and considered for crewed Mars missions include the Hall thruster which can only produce a maximum of 5 Newtons of thrust at a specific impulse of over 2600 seconds[1] while NTP has shown the capability to produce 250,000 lbf (over 1 MN) of thrust at 900 seconds[2]. It should be noted that both technologies exceed the maximum specific impulse of chemical propulsion of about 465 seconds[3]. Recent work at Analytical Mechanics Associates (AMA) has focused on estimating the mass and performance of NEP systems[4,5] alongside the development of modeling tools for NTP[5].

A NEP system is composed of multiple critical technology elements (CTEs) including the reactor, the power conversion system, the power management and distribution (PMAD) system, the electric propulsion system, and the heat rejection system. The NEP system's performance is characterized by its mass per unit electric power (specific mass) or α. The α of the NEP system and the power level both have a significant impact on the sizing of the vehicle able to complete an opposition-class mission to Mars. Design choices, such as operating temperature, and component performance metrics, such as radiator mass per area and turbomachinery efficiency, of a NEP system contribute to the α that can be achieved.

The previous research reported on the progress made with the power conversion Brayton cycle system modeled in Simulink up to the last report on this model[4]. The current updated model can now use any fluid or fluid mixture with varying concentrations as the working fluid. It can also solve for the turbomachinery parameters using a physics-based approach given desired pressure ratios and efficiencies. The parameters that are outputted are the diameters and specific speeds which can then be used to estimate the system mass in a separate model[8]. The technical problem that this present work will address is the incorporation of the turbomachinery parameters for a more accurate system mass estimation by the mass model[8].

Single and triple loop configurations of the model have been constructed that could analyze different working fluids in different loops to compare the different architectures. The solution of the model is iterative and is set to converge to a specified electrical output power level by varying the mass flow rate. Some of the components, such as the heat exchangers and recuperator, are still at a basic level with assumptions for pressure losses and efficiencies. As the model grows, the simple calculations inside the components will be replaced with more complex and rigorous ones which will replace these assumptions with a physics-based sizing approach.

A flow diagram of the single loop Simulink model is shown in Fig. 1. Energy losses of the system are listed in the red blocks, while the other blocks contain the components and

related functions.[4,5] The system thermal and pressure losses have been incorporated into the components directly.

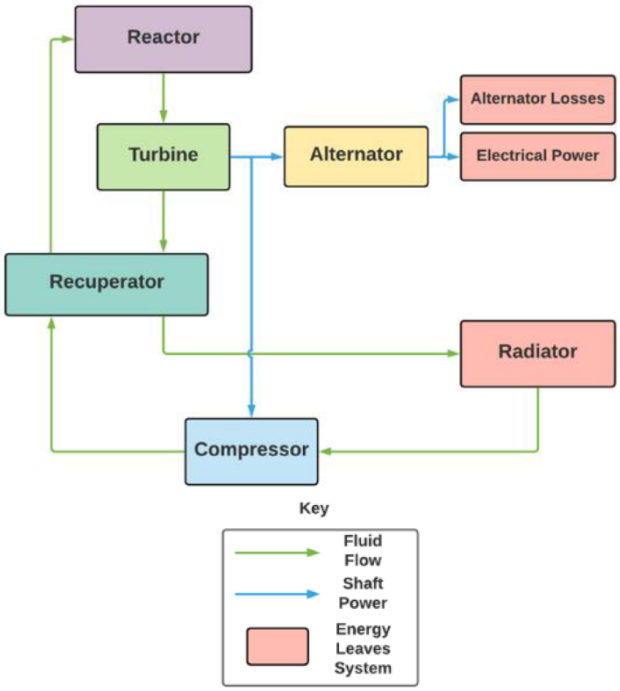

Fig. 1. Brayton Cycle Single Loop Block Diagram[4]

The triple-loop schematic of the Simulink model that uses separate working fluids in the radiator and reactor that interface with the Brayton fluid via heat exchangers is shown in Fig. 2. The turbine is responsible for producing the work required to power the compressor of the Brayton cycle, the pumps of the reactor and radiator loops, and to drive the alternator for it to generate electrical power for the electric propulsion system. Currently, the reactor is modeled with liquid lithium (Li) as a working fluid due to its high boiling point and the radiator uses sodium potassium alloy (NaK) due to its lower melting point than that of lithium. The reason that different fluids that are in the liquid state are considered for these loops is to aid in heat transfer, decrease pressure losses, and reduce the risk of a leak in the Brayton cycle. It is expected that more losses and higher required mass flow rates through the Brayton cycle will be required to produce the same electric power to the thrusters as the single loop system due to the need to power the liquid pumps and lower temperatures coming out of the heat exchangers for a given reactor outlet temperature. However, the advantages of the triple loop system are reliability/redundancy, more separable interfaces, and decreased pressure drops within the Brayton cycle. Therefore, there is a potential for a lower overall system mass with a triple-loop power cycle than a single loop. This will be examined in the mass model[8]. Future research will also analyze double-loop systems (either radiator or reactor loop augmenting the Brayton loop) and their impacts on the power conversion cycle performance as well. The following two sections will overview the equations and technical details of the added capabilities of this model. Details for the other components have been addressed in previous work[4].

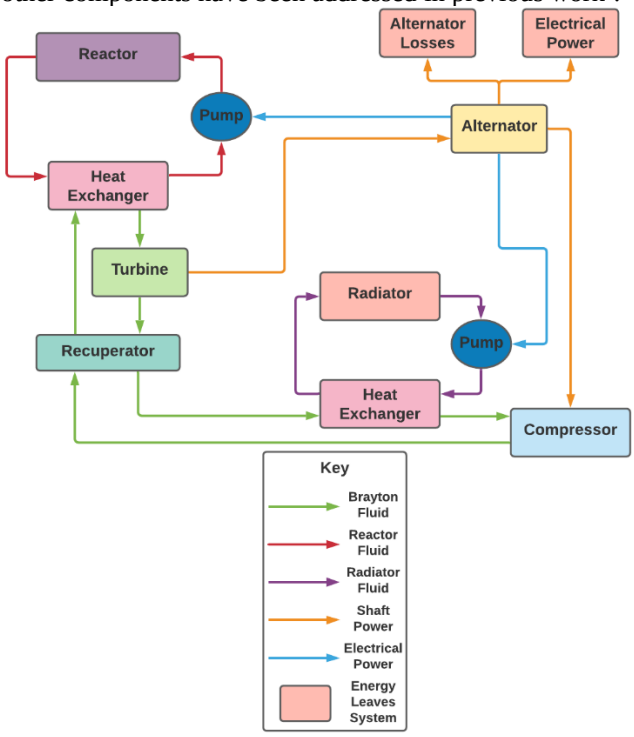

Fig. 2. Brayton Cycle Triple Loop Block Diagram

II. FLUID PROPERTIES

A change that was made since the previous modeling efforts[4,5] was the incorporation of determining the fluid properties without assuming an ideal gas mixture. The updated process involves calls to CoolProp[6] to determine the properties of the constituent species of a fluid and using the appropriate mixture formulations to calculate the mixture properties. This is done in the fluid properties code called by the function name `fluid_properties` which is used as a helper function by the model. The code was written to function as a modular extension of CoolProp, therefore, it works for both single fluid species as well as n-fluid species mixtures for selected properties. The arguments that this function accepts are listed.

Fluids (`fluids`) – this is a string array of the mixture species.

Property of Interest (`property_of_interest`) – this is the property that is requested from the function and can be as either a string or character array.

Input Property 1 and 2 Types (`in_prop1_type`, `in_prop2_type`) – since fluid properties can be determined given a set of two state values, there are two arguments that take the string or character array of the specified property call. This property call is identical to the one used by CoolProp[6]. For example, to call the specific enthalpy, the call for this property would be `'Hmass'`.

Input Property 1 and 2 Values (`in_prop1_val`, `in_prop2_val`) – the values of the property types given in the previous arguments are set in these arguments which follow their respective property types directly.

Mixture Ratio Type (`mixture_ratio_type`) (optional) – the mixture ratio type that will be assigned to the fluid mixture is provided in this argument as a string or character array for either the molar fractions `'molar'` or mass fractions `'mass'`.

Mixture Ratio (`mixture_ratio`) (optional) – the numerical values of the mixture ratio specified in the previous argument is set here as a numerical array with the elements corresponding to the fluid elements listed in the first argument. The sum of these fractions must add up to 1.

It should be noted that if a single species is set, then the last two arguments are not needed, hence they are optional, and the `fluid_properties` function defaults to using CoolProp directly. If a mixture property is requested, the function will first determine either the mass fractions from the molar fractions (Eq. (1)) or molar fractions from the mass fractions (Eq. (2)) depending on the mixture ratio type provided[7]. Both mass and molar fractions are stored as different properties and require different mixture fraction sets.

$$f_{m_j} = \frac{mw_j f_{M_j}}{\sum_{i=1}^{n} mw_i f_{M_i}} \tag{1}$$

$$f_{M_j} = \frac{\frac{f_{m_j}}{mw_j}}{\sum_{i=1}^{n} \frac{f_{m_i}}{mw_i}} \tag{2}$$

The properties that are available for mixtures that would be put into the Property of Interest argument are discussed along with their mixture formulations.

Average Mixture Molecular Weight mw_{avg} (`'M'`) – this finds the molecular weight of the mixture by using the molar fractions of the respective species as shown in Eq. (3).

$$mw_{avg} = \sum_{i=1}^{n} mw_i f_{M_i} \tag{3}$$

Specific Heat Capacity at Constant Pressure c_p (`'Cpmass'`) – The mixture mass based specific heat capacity at constant pressure uses a simple mass fraction lever rule as shown in Eq. (4). It should be noted that this formulation is invalid for cryogenic temperatures as the true formulation for the specific heat capacity at constant pressure incorporates constants from the equation of state for each respective species. However, because the temperatures within the power conversion model are higher than cryogenic (above 180 K), this simplified assumption is valid.[8]

$$c_{p_{mix}} = \sum_{i=1}^{n} f_{m_i} c_{p_i} \tag{4}$$

Specific Heat Capacity at Constant Volume c_v (`'Cvmass'`) – The mass based specific heat capacity of constant volume, just as in its counterpart, uses a simple mass fraction lever rule shown in Eq. (5) which is valid above cryogenic temperatures.[8]

$$c_{v_{mix}} = \sum_{i=1}^{n} f_{m_i} c_{v_i} \tag{5}$$

Density ρ (`'D'`) – The density of a mixture is also a simple lever rule; however, it uses the specific volume approach as that is the mass-based property that is compatible with the mixture mass fractions. Therefore, the reciprocal of the density is observed in Eq. (6). (Ref. 7)

$$\rho_{mix} = \left(\sum_{i=1}^{n} \frac{f_{m_i}}{\rho_i} \right)^{-1} \tag{6}$$

Specific Enthalpy h (`'Hmass'`) – Just as in the case of density or specific volume, the specific enthalpy uses the mass fraction-based lever rule with the formulation shown in Eq. (7). (Ref. 7)

$$h_{mix} = \sum_{i=1}^{n} f_{m_i} h_i \tag{7}$$

Specific Entropy s (`'Smass'`) – similar to the other mass fraction-based properties, the specific entropy uses a mass fraction-based lever rule shown in Eq. (8). (Ref. 7)

$$s_{mix} = \sum_{i=1}^{n} f_{m_i} s_i \tag{8}$$

Dynamic viscosity μ (`'V'`) – There are a variety of different viscosity formulations including the famous Wilke's Rule[9]. However, most of these formulations make the simplifying assumption that the diameters of the mixture species are the same. Although this is valid in the case of mixtures such as air, it is not valid for mixtures such as helium and xenon where the diameters of the species vary greatly. One correlation that does not make this simplifying assumption is Brokaw's correlation which is shown in Eq. (9) with its components defined in Eq. (10) and Eq. (11) (Ref. 10). The σ_{ij} term that appears in Eq. (9) is the sum of the radii of species *i* and *j*. Due to this correlation's inherent dependency on the molecular diameters, the Chapman and Cowling correlation for molecular diameters is used as shown in Eq. (12) (Ref. 11). Here, the molecular diameter of a species depends on that species' dynamic viscosity and temperature as dictated by the kinetic theory of gases.

$$\mu = \sum_{i=1}^{n} \frac{f_{M_i}\sqrt{\mu_i}}{\frac{f_{M_i}}{\sqrt{\mu_i}} + \sum_{\substack{j=1 \\ j\neq i}}^{n} f_{M_j} \frac{\frac{\sigma_{ij}^2}{\sigma_i \sigma_j} A_{ij}}{\sqrt{\mu_j}}} \tag{9}$$

$$A_{ij} = \mathcal{M}_{ij}\sqrt{\frac{mw_j}{mw_i}}\left[1 + \frac{\frac{mw_i}{mw_j} - \left(\frac{mw_i}{mw_j}\right)^{0.45}}{2\left(1+\frac{mw_i}{mw_j}\right) + \frac{1+\left(\frac{mw_i}{mw_j}\right)^{0.45}}{1+\mathcal{M}_{ij}}\mathcal{M}_{ij}}\right] \tag{10}$$

$$\mathcal{M}_{ij} = \left[\frac{4mw_i mw_j}{\left(mw_i + mw_j\right)^2}\right]^{1/4} \tag{11}$$

$$\sigma = \sqrt{0.1792\frac{\sqrt{k_b mwT}}{\mu}} \tag{12}$$

Thermal Conductivity K (`'L'`) – There are two popular correlations that are used to estimate the thermal conductivity of a mixture: Mason & Saxena (Eq. (13)) (Ref. 12) and Mathur (Eq. (14)) (Ref. 13). However, when compared to experimental data[14], Mason & Saxena overestimates this property while Mathur underestimates it. Therefore, an unweighted average is taken of the two correlations to "sandwich" the property and yield a more accurate value as shown in Eq. (15).

$$K_{\substack{Mason \\ \& \\ Saxena}} = \sum_{i=1}^{n} \frac{K_i}{1+\sum_{\substack{j=1 \\ j\neq i}}^{n} \frac{1.065}{\sqrt{8}}\frac{f_{M_j}}{f_{M_i}}\sqrt{1+\frac{mw_i}{mw_j}}\left[1+\sqrt{\frac{\mu_i mw_j}{\mu_j mw_i}}\left(\frac{mw_i}{mw_j}\right)^{1/4}\right]} \tag{13}$$

$$K_{Mathur} = \frac{1}{2}\left[\sum_{i=1}^{n}(mw_i K_i) + \left(\sum_{i=1}^{n}\frac{mw_i}{K_i}\right)^{-1}\right] \tag{14}$$

$$K = \frac{1}{2}\sum_{i=1}^{n}\left\{\frac{K_i}{1+\sum_{\substack{j=1 \\ j\neq i}}^{n} \frac{1.065}{\sqrt{8}}\frac{f_{M_j}}{f_{M_i}}\sqrt{1+\frac{mw_i}{mw_j}}\left[1+\sqrt{\frac{\mu_i mw_j}{\mu_j mw_i}}\left(\frac{mw_i}{mw_j}\right)^{1/4}\right]}\right\} + \frac{1}{4}\left[\sum_{i=1}^{n}(mw_i K_i) + \left(\sum_{i=1}^{n}\frac{mw_i}{K_i}\right)^{-1}\right] \tag{15}$$

III. TURBOMACHINERY ANALYTICAL FORMULATIONS

III.A. Compressors

As the fluid flows through the system, pressure losses due to powering the turbine and overcoming friction occur which need to be regained at some point. Acceleration/momentum pressure losses were not accounted because no channels with varying cross-sectional area were analyzed and the losses that would be introduced are much lower than the frictional losses. Furthermore, components that did not have a clearly defined geometry such as the recuperator, heat exchangers, and reactor use an assumed pressure loss[4]. Since the Brayton cycle fluid is not a liquid, a gas compressor must be used to increase the fluid pressure to the maximum system pressure. This maximum system pressure parameter is held constant to which the compressor must adhere. An upgrade to the Simulink model includes the utilization of a higher fidelity turbomachinery model. This enhancement allows for the knowledge of the type of turbomachinery components based on the value of their specific speed n_s and the physical diameter D. The compressor is treated as a turbine in reverse which allows the same plots to be used for both components. The type of compressor or turbine according to the specific speed value n_s is shown in Fig. 1. Because these new parameters are now incorporated, the shaft speed ω becomes an important parameter to consider. Since the compressor must adhere to the maximum system pressure, this component determines the rotational velocity of the shaft, as shown in Eq. (16). Because the fluid is gaseous, the fluid enthalpy change is used. Since the compressor increases the fluid enthalpy, the inlet enthalpy h_{in} is subtracted from the outlet enthalpy h_{out} (Ref, 15–17).

$$\omega = \frac{n_{s_c}\sqrt{\rho}(h_{out}-h_{in})^{3/4}}{\sqrt{\dot{m}}} \tag{16}$$

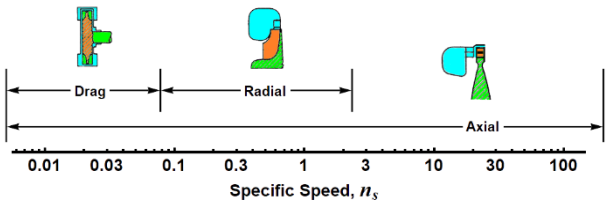

Fig. 1: Types of Turbines and Compressors According to the Specific Speed[17]

To find the compressor efficiency η_c, the contour plot shown in Fig. 2 is used. Notice that besides the specific speed n_s parameter, there is another parameter d_s which is the specific diameter. This parameter is based on the physical diameter of the component as shown in Eq. (17). An added feature to the model is that the user can either specify the physical diameter and specific speed of the compressor and have the compressor block calculate the rotational velocity and efficiency or ask the block to calculate n_{s_c} and D_c given a desired rotational shaft velocity and efficiency. The latter is done by using the least squares non-linear optimizer function or `lsqnonlin` and varying the n_{s_c} and D_c parameters until the results yield the values specified.[15–17]

$$d_{s_c} = \frac{D_c\sqrt{\rho}(h_{out}-h_{in})^{1/4}}{\sqrt{\dot{m}}} \tag{17}$$

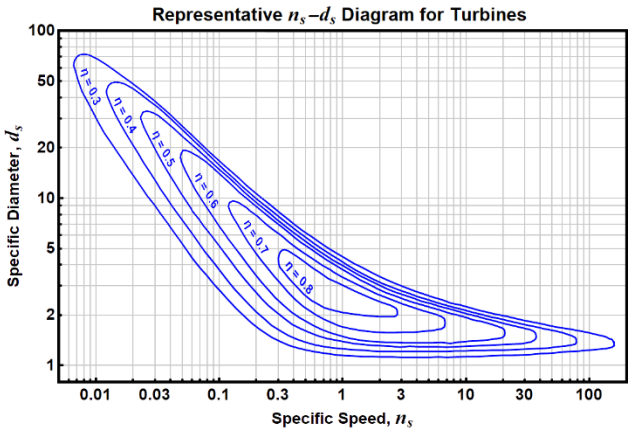

Fig. 2: Representative $n_{s_t} - d_{s_t}$ Diagram for Turbines and Compressors[17]

III.B. Turbines

The turbines are tasked with providing the mechanical work that is used by the compressor and alternator. Since the rotational velocity of the shaft is an input to the turbine and the turbine specific speed n_{s_t} is specified either by the user or by `lsqnonlin` for a given iteration, the outlet enthalpy is found as shown in Eq. (18). Eq. (18) is based on Eq. (16) but since the turbine outlet enthalpy h_{out} is less than the turbine inlet enthalpy h_{in}, h_{out} is subtracted from h_{in} in case of the turbine. Similar to the compressor, the specific diameter of the turbine d_{s_t} is calculated by using Eq. (19) to obtain the efficiency by using the contour plot in Fig. 2.

$$h_{out} = h_{in} - \left(\frac{\omega}{n_{s_t}} \sqrt{\frac{\dot{m}}{\rho}} \right)^{4/3} \tag{18}$$

$$d_{s_t} = \frac{D_t \sqrt{\rho} (h_{in} - h_{out})^{1/4}}{\sqrt{\dot{m}}} \tag{19}$$

The turbine efficiency along with the inlet and outlet enthalpies can be used to determine the isentropic outlet enthalpy h_{out_s} by using the thermodynamic efficiency equation for turbines, as shown in Eq. (20). To find any thermodynamic quantity, only two quantities must be known[18]. Since both, the inlet conditions and h_{out_s} are known, the outlet conditions are defined by linking the inlet entropy s_{in} to h_{out_s} and finding the outlet stagnation pressure $P_{0_{out}}$ from fluid property look-up tables such as CoolProp[6]. Using both h_{out} and $P_{0_{out}}$, the outlet stagnation temperature $T_{0_{out}}$ and other thermodynamic properties can be determined.

$$\eta_t = \frac{h_{in} - h_{out}}{h_{in} - h_{out_s}} \rightarrow h_{out_s} = h_{in} - \frac{h_{in} - h_{out}}{\eta_t} \tag{20}$$

Just as with the compressor, the turbine code allows the user to either specify the physical turbine diameter and specific speed or to determine these parameters automatically given a desired pressure ratio and efficiency by using `lsqnonlin`. The validation for both compressor and turbine components was performed to a surface power CO2 Brayton cycle with the results coming within 6% of that study[19].

IV. TURBOMACHINERY VALIDATION

The turbomachinery modeling approach was validated by previous work for pump and turbines in NTP applications[22,23]. Further validation was done against the NASA Fission Surface Power study which used CO2 as the working fluid[20]. Although this is not a Brayton cycle with a NEP use case, the turbomachinery modeling fidelity matches that of the present work thus yielding a better comparison than other studies[23,24]. Tables I and II show the efficiency, power, and exit temperature of the compressor and turbine, respectively, and how the present model compares to the reference. It is important to note that the compressor/turbine efficiency contour plot of Fig. 2 provides conservative values, therefore, a correction factor had to be implemented to match the efficiencies of the reference more closely for both the compressor and turbine. These correction factors scale the efficiency contour plot of Fig. 2 up by 6.42% for the compressor and up by 6.29% for the turbine. These results show that acceptable error for turbomachinery model comparison within 4% is achievable with this correction factor. Although the errors are large without this correction factor, they provide conservative estimations. These correction factors are lifted when predicting NEP power conversion parameters to provide conservative results which include a maximum turbine and compressor efficiency of 80%.

TABLE I: Compressor Validation

COMPRESSOR (Pressure Ratio = 2.065; 65,694 RPM) [20]					
Inlet Temperature (K) [20]		**Inlet Pressure (kPa)** [20]		**Mass Flow Rate (kg/s)** [20]	
360.93		330.94		0.54	
Parameter	**Reference**[20]	**Current Model**	**Difference (%)**	**Current Model (Corrected)**	**Difference (%)**
Efficiency	84.23	79.13	6.05	84.23	0.00
Power	33339.80	36173.60	8.50	33979.94	1.92
Exit Temperature	428.15	433.40	1.23	429.30	0.27

TABLE II: Turbine Validation

TURBINE (Pressure Ratio = 2.067; 65,694 RPM) [20]					
Inlet Temperature (K) [20]		**Inlet Pressure (kPa)** [20]		**Mass Flow Rate (kg/s)** [20]	
844.26		682.58		0.54	
Parameter	**Reference**[20]	**Current Model**	**Difference (%)**	**Current Model (Corrected)**	**Difference (%)**
Efficiency	86.10	80.25	6.79	86.10	0.00
Power	50285.00	47090.00	6.35	50520.00	0.47
Exit Temperature	763.71	768.90	0.68	763.40	0.04

V. SOLUTION METHOD

The previous version of the Simulink model focused on using the ODE45 solution method for a model simulation time of a single time step. The mass flow rate was kept as 1 kg/s and values per unit mass were reported. The component scaling was then assumed to be linear in terms of the power level[4]. In the present work, the case-specific mass flow rate is being calculated along with the power level and radiator area. The pressure loss inside the radiator is no longer assumed and depends on the required radiator area, duct diameter, and number of ducts. It is calculated by using the Darcy-Weisbach frictional pressure loss Eq. (21) with the Wood friction factor shown in Eq. (22).

$$\Delta P = f\frac{\rho L V^2}{2D} \tag{21}$$

$$f = 0.094\left(\frac{\varepsilon}{D_{hyd}}\right)^{0.225} + 0.53\frac{\varepsilon}{D_{hyd}} + \frac{88\left(\frac{\varepsilon}{D_{hyd}}\right)^{0.44}}{Re^{1.62\left(\frac{\varepsilon}{D_{hyd}}\right)^{0.134}}} \tag{22}$$

The mass flow rate controller inside the alternator block checks whether the desired power level is reached and adjusts the mass flow rate accordingly. The added difficulty from the higher fidelity modeling is that the initial guess for the mass flow rate must be close to the actual value. Therefore, several iterations that change this initial guess value must also be made. However, once a mass flow rate value has been established for a power level, a linear guess will result in a value that is close enough from which the system can begin convergence.

To validate this new detailed model, the previous model was used to extract the optimum turbine pressure ratio and provide an initial mass flow rate guess for the detailed model. This approach significantly saves computational time and provides an initial point of validation as the thermodynamics of the two models should not change. To perform this validation, the single loop Brayton cycle was considered, the power level was set to be constant at 1 MWe, and the radiator outlet temperature was varied. Varying the radiator outlet temperature was part of a parameter space exploration task which is presented in another paper[20]. The comparison of the efficiency, radiator area, and Brayton cycle mass flow rate outputs of both models is presented in Fig. 3. The main takeaway is that the two models mostly agree with each other. The differences are accounted for the coarse convergence of the previous model resulting in the differing values.

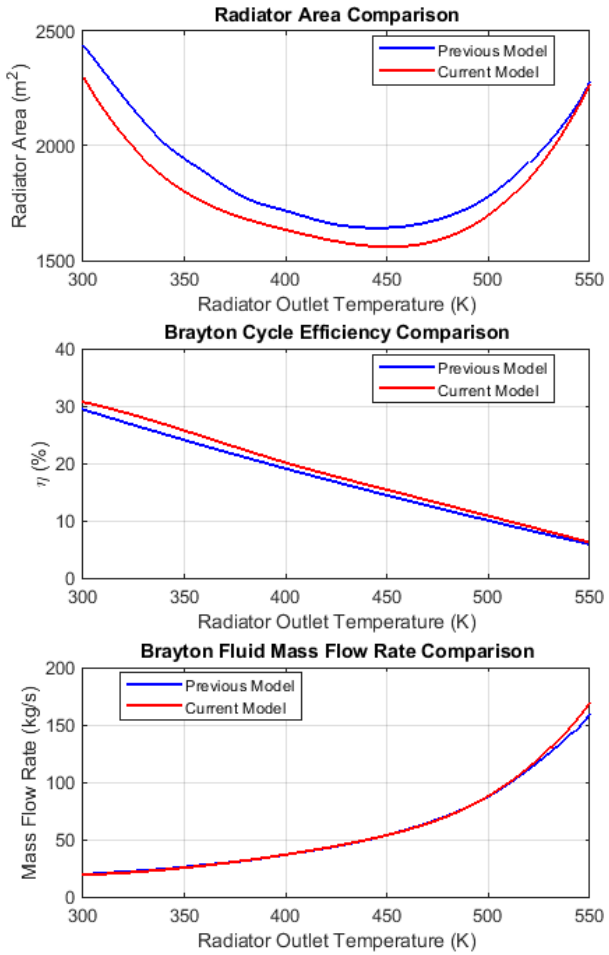

Fig. 3: Detailed Model Validation Against Simple Model

Since the purpose of the upgraded model is to gain insight into the specifics of the turbomachinery, an arbitrary power level of 1 MWe was chosen along with a low radiator output temperature of 300 K which corresponded to a turbine pressure ratio of 2.1 for the highest cycle efficiency of 32% when a compressor and turbine efficiency of 80% were assumed. All pressure losses within the system were neglected to focus on the turbomachinery performance. The rotational speed was varied, and the resulting diameter and

specific speed of both the compressor and turbine are shown in Fig. 4. Here, it is seen that the turbomachinery diameter follows a power law curve while the specific speed is linear. This is consistent with the theory of Section III within which Eq. (16) shows a linear relationship between the rotational velocity and specific speed while Fig. 2 shows the power law relation between the diameter and efficiency for a given specific speed. This shows that although increasing the rotational velocity of the turbomachinery has the potential to decrease the system mass by decreasing the disk diameters, diminishing returns are encountered and increasing the velocity further will require material reinforcement to withstand centripetal forces and thus increase the mass. Therefore, there exists a point of an optimum diameter which minimizes the system mass for a given set of parameters. The methodology for determining the turbomachinery mass is discussed in the mass model paper[20] which also provides information on the test cases and describes how this higher-fidelity model is utilized. Therefore, this paper serves as a stepping-stone for the mass model paper[20].

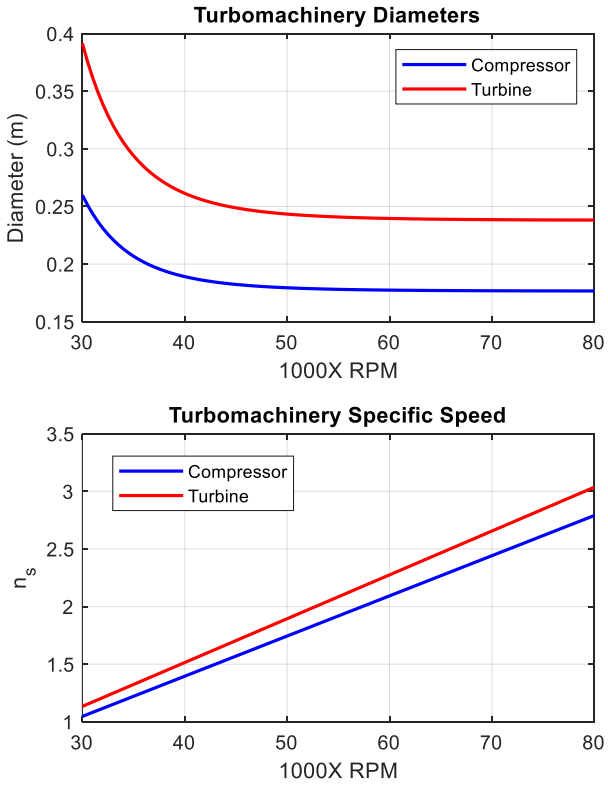

Fig. 4: Turbomachinery Diameter and Specific Speed

VI. USER INTERACTIVITY

Previous modeling work relied on the user inputting parameters into a MATLAB script file and executing different models for different cycle configurations and fluids. The workflow for the current model was upgraded and changed the user inputs from being inside a MATLAB script file into an interactive GUI in Simulink. Furthermore, the user can now see how the system operates graphically and has the capability to change the system parameters to aid convergence or to make quick comparisons. Fig. 5 shows the Input GUI where the user can freely change the species and species mixture inside the cycle without having to use a different model. Furthermore, the user can also change the specifications of the radiator and reactor loops by selecting either the Brayton fluid to enter the component directly or to interface with the component via heat exchanger and use a different fluid in the component. Moreover, this option can be changed as the model is executing so that the user can quickly see what impact changing the flow configuration does to the performance of the model.

Another option that is added is the capability to run the turbomachinery components in either pass-through mode or solve move. In the pass-through mode, the inputted physical diameters and specific speeds do not change, and the model solves for the shaft rotational velocity, turbine pressure ratio, and component efficiencies. In the solve mode, the component diameters and specific speeds are solved based on the specified shaft velocity, turbine pressure ratio, and component efficiencies. The pass-through mode will be used for transient system analysis in the future when examining off-nominal system operation.

Fig. 6 shows the output GUI where the user can see all the performance parameters of the model on one screen. This is an important feature as comparisons between turbine and compressor work levels can be made directly and the fraction of the turbine work used by the compressor can be directly seen. It is also convenient to see all the parameters in one window tab rather than in different tabs of the model. Future developments will include adding a background image to the GUI to help facilitate aesthetics and clarity regarding the grouping of parameters for each component.

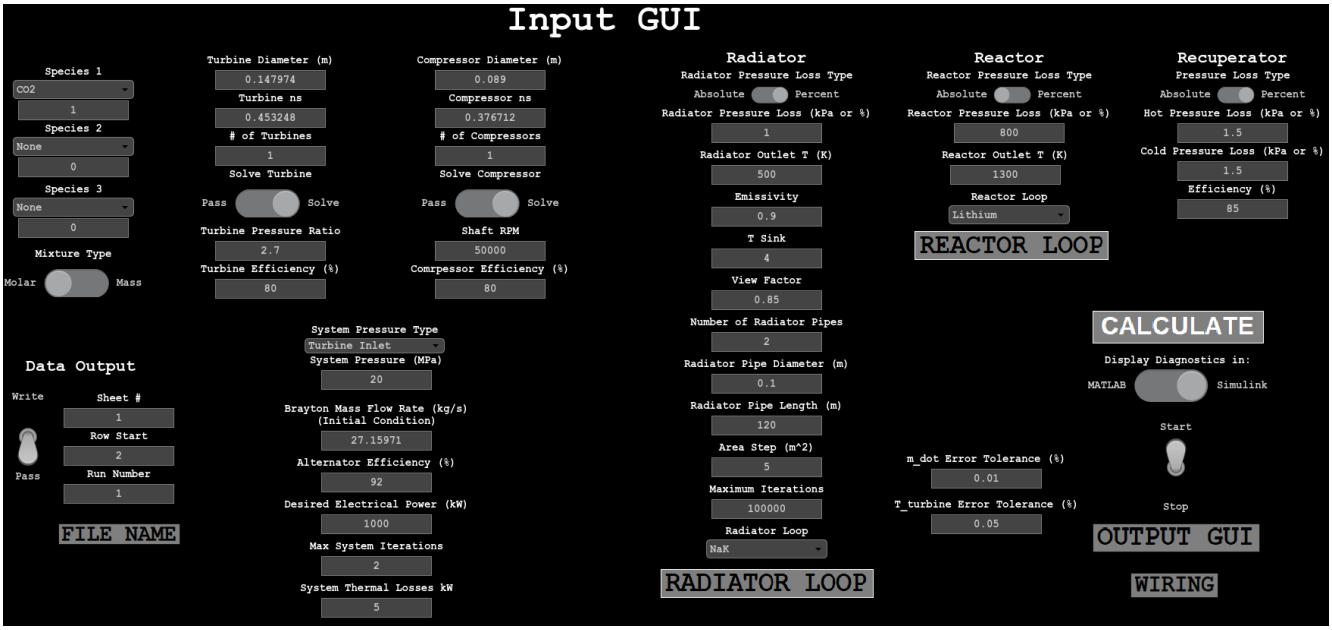

Fig. 5: Input GUI

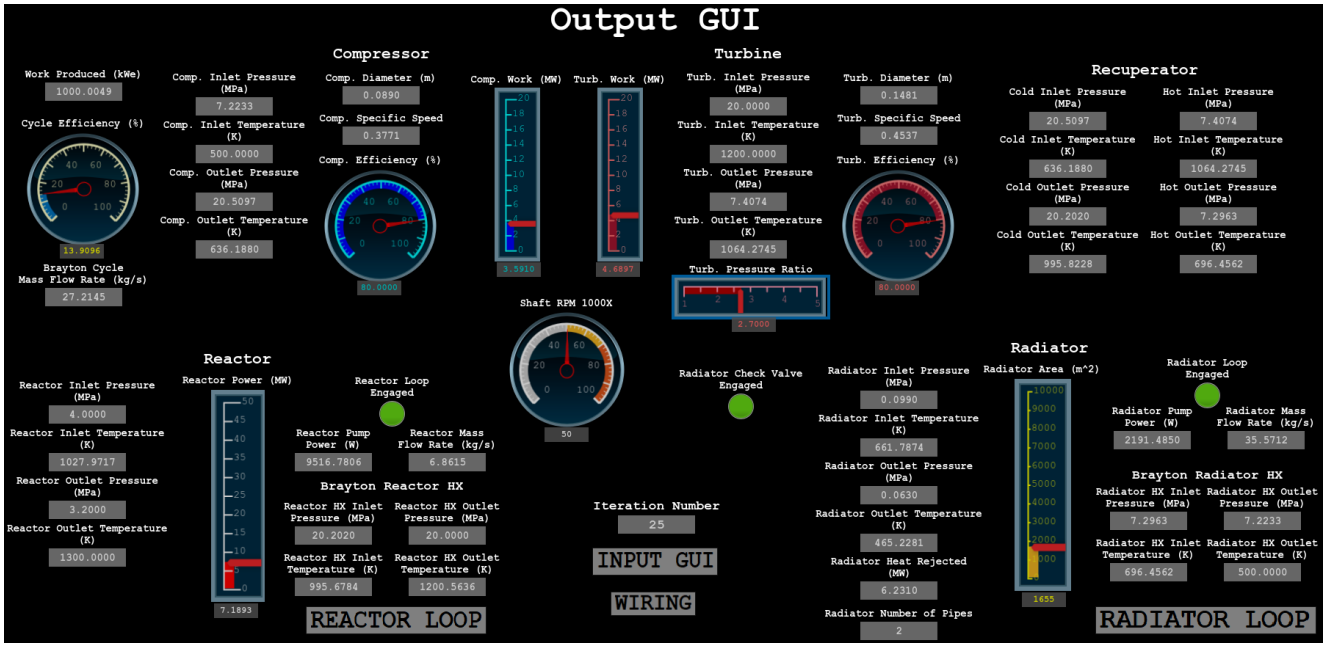

Fig. 6: Output GUI

VII. CONCLUSIONS

The Simulink model from previous work was upgraded to incorporate higher fidelity turbomachinery components, the calculation of pressure losses in the radiator, and an approach to calculate and use the actual mass flow rate for a given power level. Significant differences in the radiator area were found between this new detailed and the previous simple turbomachinery models. These differences could be attributed to the different method of finding the fluid properties and the different turbomachinery. The addition of a GUI aids the user workflow and provides new capabilities for comparison against different operational requirements. The addition of the features discussed in this work are a steppingstone for modeling the transient response of the system by providing the capability of simulating off nominal system performance.

ACKNOWLEDGMENTS

This work was supported by NASA's Space Technology Mission Directorate (STMD) through the Space Nuclear Propulsion (SNP) project. This work was funded under Contract No. 80LARC17C0003.

REFERENCES

[1] Chaplin, V. H., Goebel, D. M., Lewis, R. A., Lockwood Estrin, F., and Randall, P. N. "Accelerator Grid Life Modeling of T6 Ion Thruster for BepiColombo." *Journal of Propulsion and Power*, Vol. 37, No. 3, 2021, pp. 436–449. https://doi.org/10.2514/1.B37938.

[2] Robbins, W. H., and Finger, H. B. *An Historical Perspective of the NERVA Nuclear Rocket Engine Technology Program*. Publication NASA-CR-187154. Analytical Engineering Corporation, 1991.

[3] Aerojet Rocketdyne. RL10 Propulsion System. https://www.rocket.com/sites/default/files/documents/Capabilities/PDFs/RL10_data_sheet.pdf.

[4] Duchek, M., Clark, M., Pensado, A., Harnack, C., Machemer, W., and Grella, E. Sensitivity of Hybrid NEP-Chemical Vehicle Mass to Assumptions for Crewed Opposition-Class Mars Missions. Presented at the Propulsion and Energy Forum, Virtual Event, 2021. https://doi.org/10.2514/6.2021-3612

[5] Ducheck, M., Clark, M., Pensado, A., Harnack, C., Machermer, W., Grella, E., and Qu, M. HYBRID NEP-CHEMICAL VEHICLE AND PROPULSION TECHNOLOGY STUDY FOR CREWED MARS MISSIONS. Presented at the 68th JANNAF Propulsion Meeting, Virtual Event, 2021. https://www.researchgate.net/publication/354699389_Hybrid_NEP-Chemical_Vehicle_and_Propulsion_Technology_Study_for_Crewed_Mars_Missions

[6] Palomares, K., Harnack, C., Smith, C., Herner, R., Machemer, W., Rawlins, S., Grella, E., and Boylston, A. Nuclear Space System Analysis and Modelling (NSSAM): A Software Tool to Efficiently Analyze the Design Space of Space Reactor Systems. Presented at the Nuclear and Emerging Technologies for Space, Virtual Event, 2021.

[7] Machermer, W., Ducheck, M., and Harnack, C. Mass Sizing Study for NEP Power Conversion Concepts. Presented at the Nuclear Emerging Technologies for Space, Cleveland, OH, 2022.

[8] Bell, I. H., Wronski, J., Quoilin, S., and Lemort, V. "Pure and Psuedo-Pure Fluid Thermophysical Property Evaluation and the Open-Source Thermophysical Property Library CoolProp." *Industrial & Engineering Chemistry Research*, Vol. 53, 2014, pp. 2498–2508. https://doi.org/10.1021/ie4033999.

[9] Moran, M. J., Ed. *Fundamentals of Engineering Thermodynamics*. Wiley, Hoboken, N.J, 2014.

[10] Beattie, J. A. "The Heat Capacities of Real Gases and Mixtures of Real Gases." *Physical Review*, Vol. 34, No. 12, 1929, pp. 1615–1620. https://doi.org/10.1103/PhysRev.34.1615.

[11] Wilke, C. R. "A Viscosity Equation for Gas Mixtures." *The Journal of Chemical Physics*, Vol. 18, No. 4, 1950, pp. 517–519. https://doi.org/10.1063/1.1747673.

[12] Brokaw, R. S. *Viscosity of Gas Mixtures*. Publication NASA TN D-4496. Lewis Research Center, Cleveland, OH, 1968.

[13] Chapman, S., and Cowling, T. G. *The Mathematical Theory of Non-Uniform Gases: An Account of the Kinetic Theory of Viscosity, Thermal Conduction, and Diffusion in Gases*. Cambridge University Press, Cambridge ; New York, 1990.

[14] Mason, E. A., and Saxena, S. C. "Approximate Formula for the Thermal Conductivity of Gas Mixtures." *Physics of Fluids*, Vol. 1, No. 5, 1958, p. 361. https://doi.org/10.1063/1.1724352.

[15] Mathur, S., Tondon, P. K., and Saxena, S. C. "Thermal Conductivity of Binary, Ternary and Quaternary Mixtures of Rare Gases." *Molecular Physics*, Vol. 12, No. 6, 1967, pp. 569–579. https://doi.org/10.1080/00268976700100731.

[16] Knapp, H. "Thermal Conductivity and Viscosity Data of Fluid Mixtures (DECHEMA Chemistry Data Series, Vol. X. Part 1). VonK. Stephan undt. Hackenberger. DECHEMA, Frankfurt/M. 1989. 448 S., geb., DM 323,-." *Chemie Ingenieur Technik*, Vol. 63, No. 1, 1991, pp. 87–88. https://doi.org/10.1002/cite.330630128.

[17] Balje´, O. E. "A Study on Design Criteria and Matching of Turbomachines: Part A—Similarity Relations and Design Criteria of Turbines." *Journal of Engineering for Power*, Vol. 84, No. 1, 1962, pp. 83–102. https://doi.org/10.1115/1.3673386.

[18] Balje´, O. E. "A Study on Design Criteria and Matching of Turbomachines: Part B—Compressor and Pump Performance and Matching of Turbocomponents." *Journal of Engineering for Power*, Vol. 84, No. 1, 1962, pp. 103–114. https://doi.org/10.1115/1.3673350.

[19] Emrich, W. Jr. *Principles of Nuclear Rocket Propulsion*. Butterworth-Heinemann, Kidlington, Oxford, United Kingdom, 2016.

[20] Moran, Michael J., Shapiro, Howard N., Boettner, Daisie D., and Bailey, Margaret B. *Fundamentals of Engineering Thermodynamics*. John Wiley & Sons, Inc, 2014.

[21] Fuller, R. L. *Closed Brayton Cycle Power Conversion Unit for Fission Surface Power Phase I Final Report*. Publication NASA/CR-2010-215673. NASA, Cleveland, OH, 2010.

[22] Nikitaev, D., and Thomas, L. D. "Seeded Hydrogen in Nuclear Thermal Propulsion

Engines." *Journal of Spacecraft and Rockets*, Vol. 57, No. 5, 2020, pp. 907–917. https://doi.org/10.2514/1.A34711.

[23] Nikitaev, D., and Thomas, D. L. "Alternative Propellant Nuclear Thermal Propulsion Engine Architectures." *Journal of Spacecraft and Rockets*, 2022, pp. 1–11. https://doi.org/10.2514/1.A35289.

[24] El-Genk, M. S., and Tournier, J.-M. "Noble-Gas Binary Mixtures for Closed-Brayton-Cycle Space Reactor Power Systems." *Journal of Propulsion and Power*, Vol. 23, No. 4, 2007, pp. 863–873. https://doi.org/10.2514/1.27664.

[25] Gallo, B. M., El-Genk, M. S., and Tournier, J.-M. Compressor and Turbine Models of Brayton Units for Space Nuclear Power Systems. In *SPACE TECHNOLOGY AND APPLICATIONS INTERNATIONAL FORUM-STAIF 2007: 11th Conf Thermophys.Applic.in Micrograv.; 24th Symp Space Nucl.Pwr.Propulsion; 5th Conf Hum/Robotic Techn & Vision Space Explor.; 5th Symp Space Coloniz.; 4th Symp New Frontrs & Future Con*, No. 880, Albuquerque, New Mexico (USA), 2007, pp. 472–482.